

Ground states and magnetization process for an triangular lattice array of magnetic dots with perpendicular anisotropy

V. E. Kireev,¹ R. S. Khymyn,¹ B. A. Ivanov,^{1,2,*} and C. E. Zaspel³

¹*Institute of Magnetism, 03142 Kiev, Ukraine*

²*National Taras Shevchenko University of Kiev, 03127 Kiev, Ukraine*

³*University of Montana-Western, Dillon, Montana 59725, USA.*

(Dated: 22 ноября 2021 г.)

We analyzed the ground state of the array of magnetic particles (magnetic dots) which form a two-dimensional triangular lattice, and magnetic moment of which is perpendicular to the plane of the lattice, in the presence of external magnetic field. In the small fields long range dipole-dipole interaction leads to the specific antiferromagnetic order, where two out of six nearest neighbors of the particle have the same direction of magnetization moment and four - the opposite one. It is shown that magnetization process in such array of particles as opposed to the rectangular lattices results from the formation of the magnetized topological defects (dislocations) in the shape of the domain walls.

PACS numbers: 75.10.Hk, 75.50.Tt, 75.30.Kz

I. INTRODUCTION.

Magnetic ordering is usually attributed with exchange interaction of atomic spins, leading to rather simple magnetically ordered states.^{1,2} Long-range magnetic dipole interaction usually produces smooth non-uniformity (domain structures of different kind) above this simple exchange structure.³⁻⁵ Nevertheless, systems of magnetic moments with *pure* dipolar interaction, so-called dipolar magnets, have been theoretically studied for more than sixty years,⁶ and many physical properties, lacking in the spin-exchanged systems, are known for those models. Note first the presence of a non-unique ground state with nontrivial continuous degeneracy for quite simple bipartite lattices, like three-dimensional cubic lattice,^{6,7} and for two-dimensional square lattice,⁸⁻¹⁰ as well as specific phase transitions induced by external magnetic field.¹¹⁻¹³ Magnon spectra for dipolar magnets demonstrate non-analytic behavior either for small wavevectors,¹⁴⁻¹⁶ or at some symmetrical points within the Brillouin zone.¹⁶ The Mermin-Wagner theorem is not valid for two-dimensional magnets with a dipolar coupling of spins with continuous degeneracy, and a true long range order can exist even for a purely two-dimensional case at finite temperatures.¹⁷⁻¹⁹

The models of dipolar magnets were discussed originally in regard to real crystalline spin systems. During the last decade the most impressive achievements in magnetism were related to fabrication, investigation, and application of artificial magnetic materials, see Ref. 20 for a recent review. The nanotechnologies today have progressed to the state where the manufacture of nanosize, periodic magnetic superlattices of different types is feasible. Among them two-dimensional lattices of sub-micron magnetic particles (so-called magnetic dots) attract much attention. These magnetic dots, of different forms and of a submicron size, are made of soft magnetic materials such as Fe, Ni, Co and permalloy,²¹⁻²⁵ or highly anisotropic materials like dysprosium,²⁶ or FePt.²⁷

In the dot array lattice dots are separated from each other so that direct exchange interaction between the dots is negligible. Thus the dipolar interaction is the sole source of coupling between dots and the configuration of dot magnetic moments is dictated by the dipolar interactions of the dots and by the external field. Owing to the absence of exchange, magnetic dot arrays constitute promising material for high-density magnetic storage media. For this purposes, the dense arrays of small enough magnetic dots with the magnetic moments perpendicular to the array plane are optimal, see Refs. 28-30. Currently, ordered arrays of magnetic submicron elements have been discussed as materials for so-called *magnonics*, i.e., a new field in the applied physics of magnetism in which magnon modes with a discrete spectrum present for magnetic nanoelements are used in devices for processing microwave signals.³¹

For small enough dots with size of the order of 100 nm the magnetization inside of a dot is almost uniform, producing the total magnetic moment $m_0 \gg \mu_B$, where μ_B is the Bohr magneton, the typical value for an atomic magnetic moment. For rather small magnetic dots of volume $10^4 - 10^6 \text{ nm}^3$ the value of m_0 exceeds $10^4 \mu_B$, and for dense arrays the characteristic energy is higher than the energy of thermal motion at room temperature.^{11,12} The individual dots in an array do not touch each other, and their interaction is only determined by the dipole interaction of the magnetic moments. Therefore, magnetic dot arrays represent a new kind of magnetic material with purely two-dimensional lattice structure and high enough pure dipolar coupling between magnetic moments. Such systems represent dipolar magnets and fill their theoretical investigation with a new physical content. Thus, magnetic dot arrays are interesting as radically new objects for the fundamental physics of magnetism.

We will discuss only the situation where the magnetic moment of an individual magnetic dot is perpendicular to the array plane (xy -plane), $\mathbf{m} = \pm m_0 \mathbf{e}_z$, and the

system can be described on the basis of the Ising model. This situation is most promising for perpendicular magnetic recording systems. The energy of dipolar interaction of Ising moments perpendicular to the system's plane is minimal for antiparallel orientation of magnetic moments, that, of course, can not be fulfilled for *any* pair of particles in the array. Within the nearest-neighbors approximation, such interactions lead to antiferromagnetic (AFM) structures, e.g., simple chessboard AFM ordering is known for two-dimensional Ising square lattice with dipolar interaction.¹¹ To explain the validity of this result for real dipolar interaction it is enough to mention that accounting for next nearest neighbors gives a correction to the energy of the order of 30 % only.

Thus, the magnetic structure for square lattice dot arrays can be easily understood. However, the close-packed triangular lattices of the magnetic dots are also frequently used in experiments. In particular, these lattices of cylindrical particles considerably extended in the direction normal to the array plane are naturally obtained when the array is prepared by controlled self-organization.³² Again, the properties of these systems can be described in the two-dimensional Ising model with AFM interactions. However the triangular lattice with AFM interaction of the moments is a typical example of frustrated antiferromagnets, see for review.³³

For frustrated magnets spins interact through competing exchange interactions that cannot be simultaneously satisfied, giving rise to a large degeneracy of the ground state of the system. For nearest-neighbor Ising triangular lattice with AFM interaction, the thermodynamic properties are quite unusual.³³ It is enough to mention that in this model magnetic ordering is absent at any finite temperature $T \neq 0$; the ordering appears as a result of accounting for the next-nearest-neighbor interactions only.³⁴ This counterintuitive feature can be explained within the concept of creation of linear topological defects.³⁵ Thus, in contrast to bipartite square lattice, nearest-neighbors approximation did not provide even adequate zero approximation to the problem of the ground state of a triangular lattice.

In the present work the ground state of a triangular lattice of mesoscopic magnetic dots, each having a strong easy axis for magnetization perpendicular to the array plane, and in an external magnetic field also perpendicular to the plane of the dot lattice, will be considered. Both unbounded planar lattice and various bordered semi-infinite or finite elements of the triangular lattice are investigated. A cascade of phases with different patterns of dot magnetization has been found; these constitute the sequence of ground states as a function of the external magnetic field. In contrast to a square lattice, the transition between these states is governed by a novel mechanism involving creation of linear topological defects with non-zero magnetization.³⁷

II. MODEL DESCRIPTION.

Consider the set of Ising magnetic moments $\mathbf{m}_n = \sigma m_0 \mathbf{e}_z$, $\sigma = \pm 1$, each parallel to the z -axis, and placed in a sites of a triangular lattice \mathbf{n} ,

$$\mathbf{n} = ak\mathbf{e}_x + \frac{al}{2}(\mathbf{e}_x + \sqrt{3}\mathbf{e}_y). \quad (1)$$

where a is a lattice constant, k, l are integers, and \mathbf{e}_x and \mathbf{e}_y are unit vectors parallel to x and y axis, respectively. The magnetic moments are interacting through the magnetic dipole interaction, and an external magnetic field $\mathbf{H} = H\mathbf{e}_z$ is applied perpendicularly to the array's plane. The Hamiltonian of this system of magnetic moments can be written as

$$W = m_0^2 \sum_{\mathbf{n} \neq \mathbf{n}'} \frac{\sigma_{\mathbf{n}} \sigma_{\mathbf{n}'}}{|\mathbf{n} - \mathbf{n}'|^3} - m_0 H \sum_{\mathbf{n}} \sigma_{\mathbf{n}}, \quad (2)$$

where the first term describes dipolar interaction, with the summation performed over all of the pairs of the lattice sites. Below for the sake of simplicity we will present the energy (per one magnetic particle) in the units of m_0^2/a^3 and we will use the dimensionless magnetic field, $h = H/H_*$, where characteristic value $H_* = m_0/a^3$. The present model is clearly not restricted to a dot lattice of the type explicitly described above, but also applies directly to any triangular lattice of identical dipoles that are restricted to the two directions of normal orientation.¹⁰ It is interesting that the model formulated in this paper can be used to describe a system of a vortex state magnetic dots, accounting for the interaction of a magnetic moment of vortex cores.¹¹

As has been mentioned above, the triangular lattice is known as a typical frustrated lattice for antiferromagnetic ordering, and the frustration is present even for simplest nearest-neighbor interaction. Of course, not only nearest neighbors are important for magnetic dipole interaction. The dipole-dipole interaction is long ranged, that frequently leads to quite complicated structures with many sublattices and with high level of degeneracy. The presence of these two sources of degeneracy makes the problem less definite, and it is not obvious *a priori* what structure will constitute the ground state for such a lattice. In this situation it is natural to start with the numerical analysis of the problem.

III. GROUND STATES FOR INFINITE SYSTEM: NUMERICAL ANALYSIS

We perform Monte-Carlo analysis (simulated annealing, see for details Appendix) of the magnetic configurations with minimal energy at zero magnetic field as well as for different values of the magnetic field.

A. Simplest ground states of the system: zero field and saturation.

It is clear that for high enough magnetic field all magnetic moments will be parallel to the field, giving the saturated magnetic structure, which can be referred to as a ferromagnetic structure. The ground state of the array in the absence of magnetic field is much less trivial.

It is known that for triangular Ising lattice in the several-neighbor approximation the simple AFM order with two sublattices can be implemented.³⁸ As well, we found the same configuration for the long-range dipolar interaction in the absence of the field and for a small enough magnetic field. For these states, the magnetic elementary cell is rectangular having lower symmetry than for the underlying triangular lattice, and this state possesses much higher discrete degeneracy than the simple chessboard structure for a square lattice discussed before. Several such AFM states can occur in the system, which are different but fully equivalent in their energies. Fig. 1 presents three of these states, while the other three states are obtained from them by changing the magnetic moment sign σ_n at all of the particles. Then, we will briefly describe the magnetic state of a given particle, specifying the number of neighbors with the favorable and unfavorable orientations. The antiferromagnetic states present on the figure 1 can be called the 4-2 type state. Of all of the states of the system with the simple periodic distribution of the moments, this 4-2 type state corresponds to the *minimal* energy. It is not *optimal* because only four neighbors of the six nearest neighbors of each moment have the sign opposite to the sign of this moment, while the remaining two neighbors are parallel, and this is unfavorable to the AFM interaction. The necessity of deviation from the 6-0 optimal structure is a typical manifestation of frustration in the system.

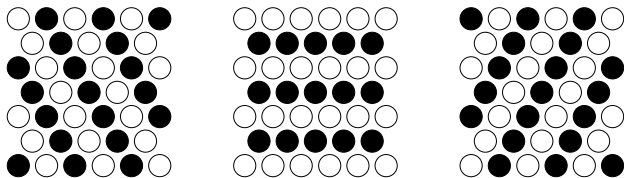


Рис. 1: Uniform states of the 4-2 type giving the energy minimum at small magnetic field. Here and below at all figures the open and closed circles denote the particles with the upward and downward moments, respectively.

B. Monte-Carlo analysis for intermediate field values.

As was mentioned above, for a zero magnetic field the simple AFM structure with zero mean value of the

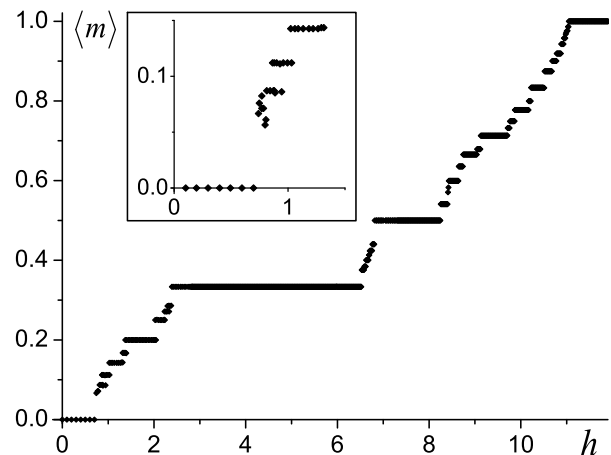


Рис. 2: Mean value of the magnetization $\langle m \rangle$ (in units of m_0 , per one dot) of the array as a function of magnetic field (in units of $H_* = M_0/a^3$) found by Monte-Carlo simulations. Detailed data at low fields are present at the insert.

magnetic moment is present. Monte-Carlo analysis shows that for some small but finite values of the magnetic field, at least up to $h = 0.7$, the mean value of the magnetic moment $\langle m \rangle$ equals zero indicating to the simple AFM structure. For higher fields, numerous more complex structures with $0 < \langle m \rangle < m_0$ occur in the intermediate region between AFM state and saturated state. The mean value of the magnetic moment (per one particle) $\langle m \rangle$ corresponding to these configurations, is present on the Fig. 2.

Note the specific regions of this dependence, present at different field intervals; first, the region with small values of $\langle m \rangle \leq 0.2m_0$ having rather non-regular dependence of $\langle m \rangle$ on h ; second, the regions with constant values of $\langle m \rangle$ independent on the magnetic field (shelves); and third, the saturation region. The characteristic magnetic structures found in these regions are depicted at the Fig. 3.

Monte-Carlo data are not too clear in the region of small fields such as 0.7-0.9, and the magnetic structures are far from the simple AFM structures, see Figs. 3(a) - 3(d), and we will discuss the magnetic structure within this region below.

1. Shelves and saturation.

Within the shelf regions, almost all initial Monte-Carlo configurations lead to the same magnetic structures, which correspond to the formation of triangular superlattices for the minority dots (antiparallel to the magnetic field) with different lattice spacings. As an example, note the ideal triangular superlattices with $\langle m \rangle = m_0/3$ and with the period $a_{s1}/a = \sqrt{3}$, see fig. 3(f) present at the values $2.4 \lesssim h \lesssim 6.4$. For higher fields, the superlattices with $a_{s1}/a = 2$ (Fig. 3(h)), $a_{s1}/a = \sqrt{7}$, (Fig. 3(i)) and $a_{s1}/a = 3$ in Fig. 3(j)) correspond to such

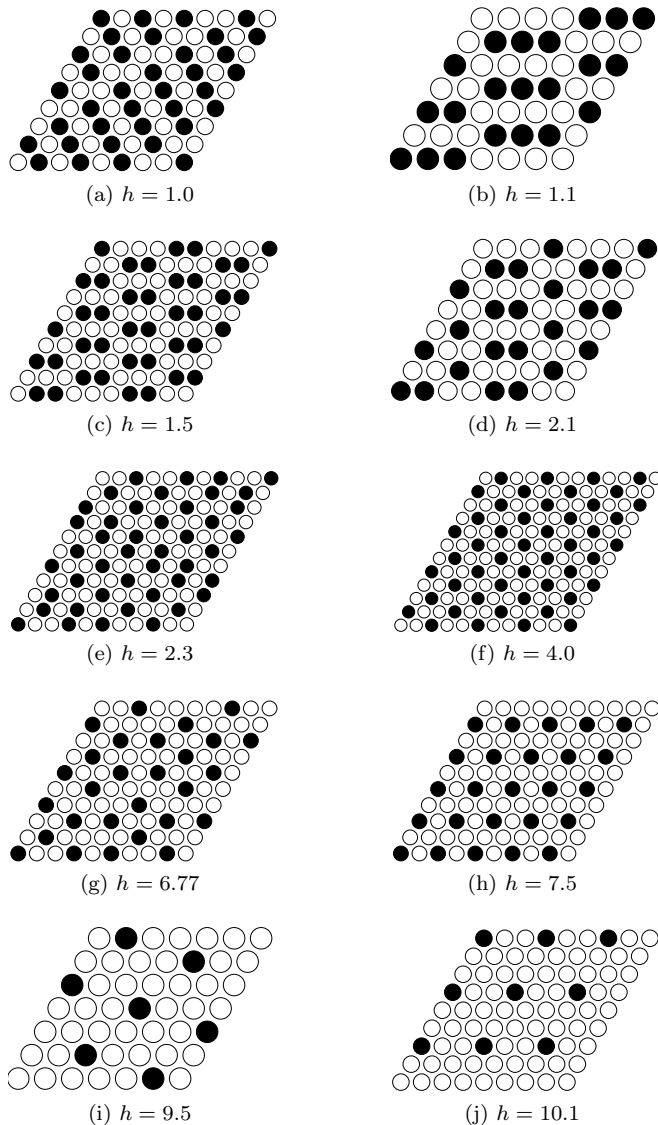


Рис. 3: Ground states for characteristic values of magnetic field found by Monte-Carlo simulations.

shelves.

For the high magnetic fields near the saturation region the magnetization process is going through the same scenario as for a square lattice, namely, by a flip of a small amount of magnetic moments and creating a superlattice of flipped dots of small density.

2. Transition region, topological mechanism.

In the region of low magnetic fields, as well as in the regions of magnetic field where the transitions between the superlattices occur, resettability of Monte-Carlo result is lowering, and the results becomes unreliable. The observed magnetic structures in these transition regions are characterized by much lower symmetry than

for the shelf regions. For example, at the values $0.9 \lesssim h \lesssim 1.5$, where the finite (but small) magnetic moment (m_0) is formed, the translational symmetry for the set of flipped dots cannot be attributed to simple superlattice structure, see Fig. 3(a). But in this figure a novel element, the additional zigzag line of the sites, oriented parallel to one of the translation vector of the lattice, is clearly seen. The resulting magnetic structure can be interpreted as an antiferromagnetic domain structure in the system, with the zigzag line as a domain wall. Such a scenario, magnetization through the creation of a set of topological linear defects, was described for a two-sublattice antiferromagnetic state with an interaction of a few neighboring moments.³⁷ For the region of small fields, the increasing the magnetic field leads to an increase of the density of the topological linear defects, see Figs. 3(b) and Fig. 3(c).

The common “topological” scenarios are present for other transition regions; both below and above the shelf regions with the magnetic structure of a form of ideal triangular superlattices of minority dots. For example, the structure present at $2.0 \lesssim h \lesssim 2.4$ can be described as a “compression” of the domains of the superlattice of period $a\sqrt{3}$ by the lines of dots with down magnetic moments, see Figs. 3(d) and 3(e), whereas the state at the opposite end of this shelf can be seen as a “rarefaction” of the $a\sqrt{3}$ superlattice, see. Fig. 3(g). The transition structures corresponding to the “higher” shelves have C_6 symmetry, higher than for low field structures. Note the essential difference of such topological behavior with what is known for a square lattice, where the competition of square and triangular (distorted) superlattices of minority of magnetic dots is responsible for magnetization processes.

C. Small fields; exhaustive search of the states.

As has been found by direct Monte-Carlo simulations, in the field region $0.9 \lesssim h \lesssim 1.5$ the ground state is realized by a system of parallel AFM stripe domains of the wight depending of the field, see Figs. 3(a) – 3(c). The minimal field for the start of this process corresponds to a low density of such defects, and to find the critical field one needs to consider larger and larger system. Namely, to present a stripe of weight n we need a system of size at least $(2n+1) \times (2n+1)$. Below in the Sec. IV we will find the starting field for the creation of the set of topological defects by an analytical calculation.

For refinement the Monte-Carlo data and for clarification of the magnetic states at the fields of interest, $0 \leq h \leq 3$, we perform the direct exhaustive search based on the picture of stripe AFM domain structures for rhombus-shaped space regions with various (not necessary equidistant) geometries of domain lines, up to the size 60×60 . It appears that for all fields the only equidistant structures corresponds to the minimal configurations, with linear system of stripes at $h < 1.5$

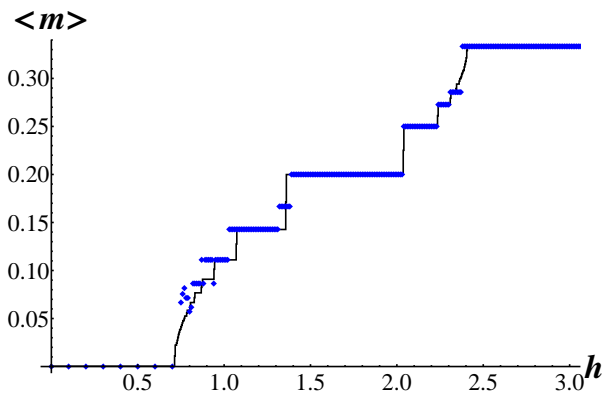


Рис. 4: Magnetization function at low fields found by exhaustive search of the states of rhombus-shaped samples (full line) and the Monte-Carlo data (symbols).

or triangular superlattice at $h > 2.0$. Then the only equidistant structures with the size up to 300×300 were examined. The magnetization curve based on these calculations is represented in the Fig. 4 and compared with the Monte-Carlo data.

IV. MAGNETIC GROUND STATES: ANALYTIC DESCRIPTION.

As has been found in the previous section, for small values of the magnetic field, the magnetic moment equals zero corresponding to the simple two-sublattice AFM structure, whereas for high magnetic field the saturated magnetic structure, or ferromagnetic structure, is present. It is known that for a non-frustrated square lattice of Ising magnetic moments the destruction of both types of the magnetic order is started through creation of the point defect in the state, the single magnetic dot with the magnetic moment reversed with respect to the regular structure of a given state.¹¹ First, in this section we will check the validity of such scenarios for ferromagnetic and AFM states of triangular lattice array of magnetic dots. Then the theoretical description of the novel topological mechanisms will be obtained.

A. Point defect scenarios.

In order to determine the values of the magnetic fields which correspond to such “point defect instability” we have calculated the change in dipolar interaction energy that occurs when the magnetic moment of a single dot is reversed with respect to the ferromagnetic and two-sublattice AFM structures. This energy change is determined by the energy per dot in the initial states,¹¹ which can be expressed by simple lattice sums calculated with high precision. These sums here and below were calculated with standard program package *Mathematica*.

1. Saturation.

The point defect scenario describes well the instability of the saturated state. It is easy to see that the change of the energy of the saturated state with the flip of a single magnetic moment can be presented as

$$W_1 = 2m_0(H - H_{\text{sat}}), \quad (3)$$

where

$$H_{\text{sat}} = m_0 \sum_{\mathbf{n}_i \neq 0} \frac{1}{|\mathbf{n}_i|^3} \equiv h_{\text{sat}} \frac{m_0}{a^3}, \quad h_{\text{sat}} \approx 11.034176. \quad (4)$$

The quantity H_{sat} determines the saturation field for a triangular lattice of Ising magnetic moments. If the magnetic field $H < H_{\text{sat}}$, the value of W_1 is negative and the flipping of a dot becomes favorable. The value h_{sat} is higher than for a square lattice, $h_{\text{sat}}^{\text{square}} = 9.034$, which just reflects the higher density of the triangular lattice comparing with the square lattice. Note here that the accounting for only nearest-neighbor interaction gives a much lower value $h_{\text{sat}}^{\text{NN}} = 6$ clearly demonstrating the importance of the long range character of magnetic dipole interaction for the description of the ferromagnetic state.

The energy of the simultaneous flip of a pair of magnetic moments placed at the distance $|\mathbf{n}|$ can be easily written as

$$W_2 = 2W_1 + 4m_0^2/|\mathbf{n}|^3, \quad (5)$$

that can be interpreted as a repulsion of the flipped dots.

Evidently, for $H < H_{\text{sat}}$ some magnetic moments tend to reverse, and the creation of a finite density of reversed magnetic moments becomes favorable. The flipped dots should be dispersed as far from each other as possible, in order to minimize the energy of their repulsion. Thus one would expect these flipped dots to be organized in a triangular superlattice, with the lattice spacing a_{sl} . We can regard the resulting system as the superposition, on the original triangular lattice with magnetic moment $+m_0$, of the triangular superlattice of “double dots” of moment magnetic moment $-2m_0$. From this simple picture, it is clear that the mean value of the magnetic moment per one dot $\langle m \rangle$ can be expressed through a_{sl} as following, $\langle m \rangle = m_0 - 2m_0(a/a_{\text{sl}})^2$.

This picture also allows us to present the energy of dipolar interaction of the array with a small density superlattice through the known value of h_{sat} , see Ref. 11. First, note that the flipped (double) dots experience the field H_{sat} from the rest of array. Consequently the interaction energy of the triangular lattice and superlattice is $2m_0\varepsilon H_{\text{sat}}$, $\varepsilon = (m_0 - \langle m \rangle)/m_0$, per one dot of the full lattice. Then the contribution to the energy of each double dot due to its interaction with all other double dots equals to $(1/2)h_{\text{sat}}(2m_0)^2/(a_{\text{sl}})^3$, per one double dot. This contributes $4W_{\text{FM}}(a/a_{\text{sl}})^{5/2}$ to the mean dipolar energy per one dot of the overall lattice. Combining all these contributions and adding the

Zeeman energy W_H , $W_H = -\langle m \rangle H$, we can obtain the approximate formula for the energy of the superlattice state per one dot in the form

$$W = \frac{m_0^2}{a^3} \left[\frac{h_{\text{sat}}}{2} - h + \varepsilon (h - h_{\text{sat}}) + 2h_{\text{sat}} \left(\frac{\varepsilon}{2} \right)^{5/2} \right]. \quad (6)$$

Minimizing the energy (6) over $\langle m \rangle$ (in fact, over ε) yields

$$\frac{\langle m \rangle}{m_0} = 1 - 2 \left(\frac{2(h_{\text{sat}} - h)}{5h_{\text{sat}}} \right)^{2/3}. \quad (7)$$

This dependence describes very well the numerical data for the dependence $\langle m \rangle$ on H near the saturation, which can be fitted by the dependence common to (7), with the power 0.656 instead of $2/3 \simeq 0.667$, and with the coefficient 1.087 instead of $2(2/5)^{2/3} \simeq 1.086$. Thus the point defect scenario based on the reversal of a single magnetic moment describes well the instability of the saturated state for both triangular and square lattices.

2. Low fields.

In principle, the common calculations can be performed for AFM state, as well as for any state with the superlattice of flipped dots of the same symmetry as for underlying dot lattice. This approach describes well the instability point for the AFM state for a square lattice of magnetic dots.¹¹ Let apply it to our triangular dot lattice. Reversing the magnetic moment of one dot in the AFM state becomes favorable at $H \geq H_{\text{AFM}} \equiv 2E_{\text{AFM}}/m_0$, where

$$H_{\text{AFM}} = \frac{m_0}{a^3} \sum_{k,l \neq 0} \frac{8}{[3(2k+1)^2 + (2l+1)^2]^{3/2}} - \frac{m_0}{a^3} \sum_{k,l \neq 0} \frac{1}{[3k^2 + l^2]^{3/2}} = 1.8377 \frac{m_0}{a^3} \quad (8)$$

This value is much higher than the instability field $h \simeq 0.7$ found numerically in the previous section. Thus the reversal of a single magnetic moment cannot describe the instability of the AFM state for triangular lattice.

B. Instability of AFM state through creation of topological line.

As we found by Monte-Carlo analysis, the AFM state loses its stability as the field increases because of the creation of topological defect lines. These lines can be also called domain walls, because within the description of AFM structure in terms of the standard antiferromagnetic order parameter (antiferromagnetism vector $\mathbf{L} = \mathbf{m}_1 - \mathbf{m}_2$, where \mathbf{m}_1 and \mathbf{m}_2 are the magnetic moments for different sublattices) the values of \mathbf{L} have different signs on both sides of this wall. This defect line

corresponds to an additional zigzag line of the particles with magnetic moments, which are oriented as their neighbors, and should be normal to one of the elementary translation vectors, see Fig. 5.

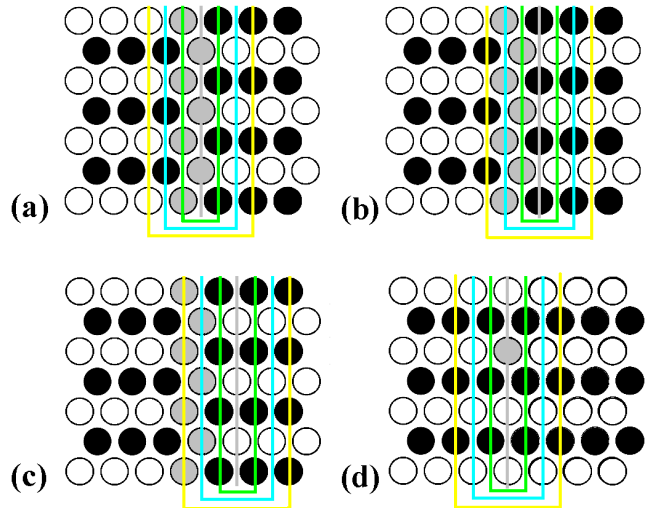


FIG. 5: (color online). (a) - (c), the structures for topological defect; (d) the ideal AFM structure; the characteristic lines used for calculation of the defect energy are shown, see details in the text. As usually, the open and closed circles denote the particles with the upward and downward magnetic moments, respectively, but the dots with upward magnetic moments within the defect line are mentioned by grey.

An importance of defect lines for thermodynamics is a well-known property of two-dimensional systems with discrete symmetry breaking. Because of the creation of a finite density of such lines, the long range order is destroyed at finite temperature, determined by the energy of the defect, see, for example, the article.³⁵ But for frustrated AFM states the behavior can be very unusual. In particular, the magnetic order for AFM Ising system with the nearest-neighbors interaction is absent at any finite temperature $T > 0$.^{33,34} Generally, this behavior can be explained using the defect line picture of the phase transition, with the vanishing of energy (more exactly, the free energy) of a certain linear topological defect. For triangular lattice Ising model with nearest-neighbor interaction it could be linear twin boundary defects, which separate the different states presented in Fig. 1.³⁵ Examples of these states appear for finite systems, see below Sec. VI and figures wherein. The formation of these defects does not violate the 4-2 relation. Thus their energy is zero in the nearest-neighbor interaction approximation and should be positive but small for dipolar coupling.

For our system of mesoscopic magnetic particles with a dipole interaction, the effect of a magnetic field, instead of thermal effects, should be significant. The topological defect line with non-zero magnetization was recently found.³⁷ This defect coincides with that observed in our

numerical simulations, compare Fig. 5 and Figs. 3(a) - 3(d) above. The particles directly entering into the defect line have an unfavorable configuration of the 3-3 type, and their presence results in energy loss; however, they are adjacent to the particles (with the downward magnetic moment) having a 5-1 configuration more advantageous than the standard 4-2 configuration. The numbers of these anomalous states coincide with each other. Thus the creation of this wall does not result in energy loss in the system in the nearest-neighbor approximation, and the loss should be small for particles with dipolar coupling. In contrast to twin boundary defects considered before,³⁵ this domain wall has a nonzero magnetic moment. As a physical consequences of this property note that the behavior of the system in a magnetic field is dictated by the defects with nonzero magnetic moment. In fact, for such a defect the additional energy gain m_0H per defect particle appears in the magnetic field H . Then the defect energy decreases as the field increases and becomes zero at $H = H_{\text{DW}} \equiv E_{\text{DW}}/m_0$. Then for $H \geq H_{\text{DW}}$ the finite density of such defects will be present in the ground state. This is exactly the scenario observed in our numerical simulations at magnetic field at the range 0.7 - 1.5.

In order to find the critical value of the field H_{DW} , let calculate the energy of the domain wall E_{DW} . It is convenient to use the symmetry of the state with the defect line and to divide the full lattice into lines of dots parallel to the defect line, as it is shown in the Fig. 5. It is evident that all dots within one such line have the same energy, and the energy of the domain wall (per one dot in the defect line) can be present as a sum over these lines as following

$$E_{\text{DW}} = -\frac{1}{2} \sum_n m_0 \sigma_n H_n \quad (9)$$

where the integer n describes the distance a_n of the given line from the defect line, $a_n = an/2$, $\sigma_n = \pm 1$ gives the sign of the moment for the n -th line, and H_n is the magnetic field created on the dot in the n -th line by other dots in the system. To find the field H_n it is convenient to group all other dots to pares of lines, equidistant from the n -th line, as it is shown for $n = 0, 1, 2$ at Fig. 5, (a), (b) and (c), respectively. Let us enumerate these pairs by an integer k so that distance between n -th line and one component of the k -th pair equals to $ak/2$, the pairs with $k = 1, 2, 3$ are present at the Fig. 5. Then the energy of the magnetic state with a domain wall can be presented by a double sum, over $n > 0$ and $k > 0$.

It is easy to see that for any finite n the only pairs with limited $k < n$ contribute to the energy of the state with the domain wall. For example, for the lines directly entering the defect line [$n = 0$, see Fig. 5 (a)] the contributions of two lines composed any pair cancel each other. For this line, the non-zero contribution to the energy is given by the dots from the same line, denote this contribution as ε_0 . Then, for the line with $n = 1$, only one pair gives non-zero contribution, see Fig. 5 (b),

and the energy can be written as $\varepsilon_0 - 2\varepsilon_1$. Similarly, for $n = 2$ the energy is $\varepsilon_0 - 2\varepsilon_1 + 2\varepsilon_2$, see Fig. 5 (c), and so on. Finally, the energy of the state with domain wall is presented through ε_0 and the particular finite sums of the positive quantities ε_n ,

$$\begin{aligned} \varepsilon_{2n+1} &= \sum_{k=1}^{\infty} \frac{4}{[(n+1/2)^2 + 3(k-1/2)^2]^{3/2}}, \\ \varepsilon_{2n} &= \sum_{k=1}^{\infty} \frac{4}{(n^2 + 3k^2)^{3/2}} + \frac{2}{n^3}. \end{aligned} \quad (10)$$

The energy of the domain wall equals the difference of the energy of the state with the domain wall and the ground state energy. To find the ground state energy, it is convenient to use the same presentation by the parallel lines, see Fig. 5 (d), and to present it by the same sums ε_n . It is clear that the energy per one dot in any line in the ground state is proportional to an infinite sum of the form $\varepsilon_{\text{GS}} = \varepsilon_0 + 2 \sum_{n=1}^{\infty} (-1)^n \varepsilon_n$. Then the domain wall energy can be found by term-by-term summation of corresponding contributions of the form $[(\varepsilon_0 - \varepsilon_{\text{GS}}) + (\varepsilon_0 - 2\varepsilon_1 - \varepsilon_{\text{GS}}) + \dots] \equiv h_{\text{DW}} = 2\varepsilon_1 - 4\varepsilon_2 + 6\varepsilon_3 + \dots$. The corresponding infinite series $h_{\text{DW}} = -2 \sum_{n=1}^{\infty} (-1)^n n \varepsilon_n$ are sign-alternating and converges quite well. Finally, domain wall energy per one dot E_{DW} can be presented as follows

$$E_{\text{DW}} = m_0 H_{\text{DW}}, H_{\text{DW}} = h_{\text{DW}} \frac{m_0}{a^3}, h_{\text{DW}} = 0.70858944. \quad (11)$$

Here we also present the characteristic value of the magnetic field, and $H_{\text{DW}} = E_{\text{DW}}/m_0$ determining the border of stability of the simple AFM state; for $H > H_{\text{DW}}$ AFM state becomes unstable against creation of domain walls. Note the calculated value (11) is in good agreement with that found by numerical simulations, but it is much lower than the field of point defect instability for AFM state, $H_{\text{AFM}} = 1.8377m_0/a^3$.

C. Plateau description

Monte-Carlo simulations result in some peculiarities (See Fig. 6) in the dependence of the magnetization on applied magnetic field in the form of plateaus, where the value of the function does not change over a wide range of the argument.

These peculiarities have a simple explanation. The magnetization of the array increases at small external field due to the formation of parallel topological defects in the form of domain walls. At some critical concentration of such walls the resulting state in nothing but the superlattice of flipped dots which has the triangular structure that coincides with the array symmetry; See Fig. 3(f,h,i,j). Such a superlattice transforms into the structure similar to itself but with the other step (lattice constant) as the applied field increases. Since the lattice constant has discrete

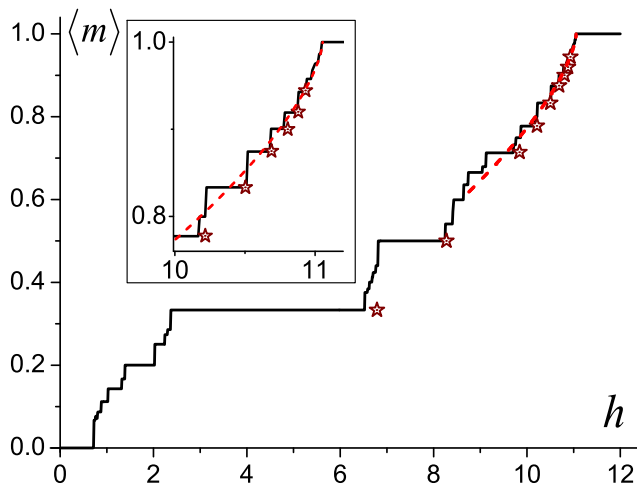


Рис. 6: (color online) The magnetization function dependence on external magnetic field. Numerical data are present by solid line, analytical calculations of the instability points specified by the symbols, see Eq. 13.

values $a_{sl}/a = \sqrt{3}, 2, \sqrt{7}, 3, 2\sqrt{3}, \sqrt{13}, 4, \sqrt{19}, \sqrt{21}, 5, \dots$, then such superstructure has good stability against the alteration of the external field and magnetization can be changed only stepwise. One can see that such a structure consists of two inversely magnetized ferromagnetic states with the lattice constants a and a_{sl} . As stated above the magnetization of a such state is

$$\langle m \rangle = m_0 - 2m_0(a/a_{sl})^2. \quad (12)$$

The value of the field of the stability loss of such superstructure relative to the transition to other lattice constant can be easily calculated on the same principle as the field of the ferromagnetic state stability that was done above.

$$H_{sl} = h_{sat} \frac{m_0}{a^3} \left[1 - 2 \left(\frac{a}{a_{sl}} \right)^3 \right], \quad (13)$$

where the multiplier 2 in the numerator responds to the change of magnetization of the dot in comparison with the ferromagnetic state and $h_{sat} = 11.034176$ is the field of the transition to the saturated state. The values of these fields depending on the superlattice magnetization are represented by symbols (stars) on the Fig. 6.

As was found by numerical simulations, the destruction of such superstructures can go through the creation the lines of topological defects, see Fig. 3(g). This mechanism assumes that unit cells of the superlattice repel themselves with an increase of the field and the line of the dots magnetized inversely to the dots of the superlattice passes between them. The situation recurs until a new superlattice formes with a larger lattice constant. Though this effect occurs in the narrow range of the field it leads to instability of the superlattice at

smaller value of the field than is predicted in equation (13).

Formation of the triangular superlattice is impossible at small values of the applied magnetic field $h \leq 2.5$ but some rectangular superlattices with C_2 -symmetry are possible, see Fig. 3(c), which also are the reason for the plateaus appearance (but not so well pronounced) at the magnetization function, see Fig. 4.

V. SEMI-INFINITE ARRAYS: THE ROLE OF THE BOUNDARIES.

In the previous theoretical consideration we analyze the idealized model of the infinite array. Of course, real superstructures are large, but finite systems. The border elements (edge surface of an array) are expected to play a considerable role in the formation of the properties of the ground state. The existence of any translational invariance significantly simplifies the problem. For finite system, there is no translational symmetry. The finiteness of the system manifests itself in two different ways; first, through the difference in the coordination numbers for the dot at the border and in the bulk; and second, by the direct influence of the system size. In this sections, we will analyze the “border problem” only, assuming that the array is semi-infinite, e.g., it is bordered by one border line. As well we will discuss the “edge problem”, investigating the properties of an edge element, a single dot located at the crossing of two borders. The systems of finite size will be considered in the next section, mainly numerically. We primarily will discuss only the simplest geometry of the system, supposing that the array’s borders are parallel to simplest translation vectors of the underlying triangular lattice.

A. Analytical description

Consider the simple two-sublattice AFM state typical for an array at small enough magnetic fields. For an infinite array, any magnetic dot is influenced by the magnetic field, generated by other dots of the array. This field is parallel to the dot’s magnetic moment; and the strength of the field is given by the expression $h_{AFM} = 1.8377$.

Let consider some different kinds of bordered arrays. It is clear that the same quantity, the dipole magnetic field at a dot located near the border, determines the stability of the state. In order to calculate the field on a given dot, it is convenient to take the coordinate system with the origin at this dot, see Fig. 7. For all cases of interest, namely, for a magnetic dot located at the edge of the array or at one of its borders of different orientation, a certain common property is easily seen. The magnetic field acting at the dot can be expressed in terms of auxiliary sums, from the single sums over dots located at the ray beginning at the coordinate origin (half the

coordinate axis) and a few double sums over dots located in one of the array sectors that is shown in Fig. 7. Then for concrete estimates we will chose the dot at the origin with the “down” magnetic moment, so a negative value of the field corresponds to stability of the configuration and a positive value of the field corresponds to the instability of the state.

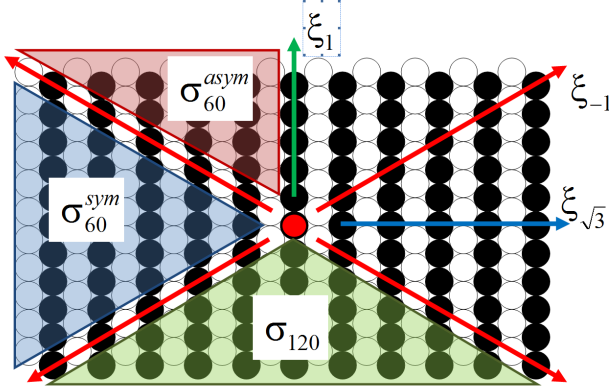


Рис. 7: (color online) The definition of auxiliary sums used for analysis of semiinfinite arrays in AFM state, see the text.

The single sums are expressed in terms of the Riemann $\zeta(3)$ - function,

$$\begin{aligned}\xi_1 &= \sum_{n=1}^{\infty} \frac{1}{n^3} = \zeta(3) = 1.20206, \\ \xi_{-1} &= \sum_{n=1}^{\infty} \frac{(-1)^n}{n^3} = -3\zeta(3)/4 = -0.90154, \\ \xi_{\sqrt{3}} &= \sum_{n=1}^{\infty} \frac{1}{(3n^2)^{3/2}} = \frac{\zeta(3)}{3\sqrt{3}} = 0.23134,\end{aligned}\quad (14)$$

whereas the double sums can be easily determined numerically, for example,

$$\sigma_{60}^{asym} = \sum_{n=1}^{\infty} \sum_{k=1}^{\infty} \frac{(-1)^n}{[n^2 + kn + k^2]^{3/2}} = -0.22164 \quad (15)$$

$$\sigma_{60}^{sym} = -\frac{1}{2} [h_{AFM} + 4\sigma_{60}^{asym} + 4\xi_{-1} + 2\xi_1] = 0.12545. \quad (16)$$

Using a simple geometrical consideration, all the double sums of interest can be expressed through the value of $h_{AFM} = 1.8377$ and the partial sum σ_{60}^{asym} found above. The knowledge of this particular sums gives the possibility to determine the stability of any particular dot of interest.

Let us start with the infinite borders parallel to the elementary translation vector. There are two kinds of such a border, with all magnetic moments parallel and with the alternating magnetic moments, see Fig. 7. The

magnetic field on the dot in these borders, $h_{\uparrow\uparrow}$ and $h_{\uparrow\downarrow}$, respectively, can be written as

$$\begin{aligned}h_{\uparrow\uparrow} &= \xi_1 - h_{AFM}/2 = 0.2832, \\ h_{\uparrow\downarrow} &= \xi_{-1} - h_{AFM}/2 = -1.8204.\end{aligned}\quad (17)$$

Note first that $h_{\uparrow\uparrow}$ is positive, and the infinite borders with parallel magnetic moments is unstable in the absence of the magnetic field, such a fragment can appear at some finite value of the magnetic field only. Both the aforementioned properties are in agreement with the numerical analysis of finite arrays, see the next section. In particular, the border with parallel magnetic moments never appears for finite arrays; instead, the complicated multi-domain AFM structure is present. It is worth noting an essential difference in behavior between triangular and square lattices. In the latter case, the simple AFM state with C_4 -symmetry (chessboard AFM) is the ground state for finite systems with any shapes of the array including the systems with acute angles or for system of circular shape.¹² In contrast, the “perfect” AFM ordering with C_2 -symmetry for the triangular lattice is possible only for rhombic shape of the sample, borders of which are parallel to the fundamental translation vectors of the lattice. Lines which consist of unidirectional dots would have sharp bends in all other cases, See Section VI.

The next point of interest is the behavior of the magnetic dot with the downward magnetic moment at the edge of the array in the AFM state. For a square lattice, the magnetic moment of such dots becomes unstable at the magnetic field that is much weaker than the instability field for the infinite system, $h_{edge}^{square} = 1.563$. Further, the magnetic moment of this dot is reversed at this value of the field. For a square lattice, such reversal of the edge dot is the beginning of the destruction of the AFM state in the finite array. For the triangular lattice, the edges of finite array are also a “weak points” for a single-dot instability. The values of the instability field for a dot at the vertex of edges with the angles 60° and 120° , can be expressed through the sums σ_{60}^{sym} and σ_{120} , respectively. The state of the edge dot is then stable and does not change until the external field increases to the value. The field h_{60} of the reversal of the single dot at the vertex of 60 -degree edge can be present as

$$h_{60} = -(\sigma_{60}^{sym} + 2\xi_{-1}) = 1.67764, \quad (18)$$

whereas for 120 -degree edge the instability field h_{120} has the lower value,

$$h_{120} = -(2\sigma_{60}^{asym} + \xi_1 + 2\xi_{-1}) = 1.0443 \quad (19)$$

Thus we found that the more sharp edge appears to be more stable against the action of the magnetic field (note that for square lattice the situation is opposite¹²). This result seems to be a contra-intuitive, but it is the reflection of the frustration for AFM state at the triangular lattice.

The above field for single-dot edge and border instability are weaker than the instability field for the border of infinite system $h_{\uparrow\downarrow} = 1.82039$ but their values are higher than the value $h_{DW} = 0.7085$, where the creation of the domain wall becomes favorable. Thus, the scenario with the creation of such domain walls is preferable in a thermodynamic limit. On the other hand, the creation of a topological domain wall require the perturbation with a reversal of an essential number of dots (formally, proportional to the system area). Thus such a process needs the overcoming of a very high (formally, infinite) potential barrier, and it is hard to realize it for a real experiment.

To find an alternative scenario, let us consider the domain wall which pass nearby the 120-degree corner. Thereto we fix the corner site to the origin of coordinates and build y -axis on the bisector of the angle, see insert on the Fig. 8. Then the domain wall which lays at the distance y_{DW} results in the magnetization flip-over, in comparison with the ground state, on all sites left from the wall. Single dot on the vertex angle is equivalent to the domain wall with the coordinate $y_{DW} = 0$. We calculated the necessary field of such a domain wall appearance for different y_{DW} , see Fig. 8. Calculations were carried out by the direct summation of the array energy, which consists of 400 lines in the y direction.

As one can see from the the data on Fig. 8) the necessary field is higher for the domain wall near the corner of the array than for the deep-laid wall. Also, we can see from the figure that the field of the domain wall generation depends on the relative directions of the applied magnetic field and the magnetization of the vertex site (taken, as before, negative on the figure). Thus only domain walls with integer values of y_{DW} are of interest for the problem. With an increase of y_{DW} the field that is required for the wall formation decreases converging exponentially to the field of creation of infinite wall, that is similar to the presence of the potential barrier on the surfaces of solid. Therefore one can assert that the smaller the difference between applied field and $h_{DW} = 0.7085$ the farther from the corner domain wall appears.

It is necessary to take into account for large arrays that domain wall at the sufficient distance $|y|$ from the site produces the magnetic field at this site proportional to

$$\int_0^{\infty} \frac{dx}{(x^2 + y^2)^{3/2}} = \frac{2}{y^2}, \quad (20)$$

notably converges to zero when $|y| \rightarrow \infty$. Therefore, the formation of the another deep lying domain wall is more energetically favorable than the wall near the corner for the small concentration of topological defects. And consequently the magnetization of the large arrays increases firstly in the volume, where equilibrium density of parallel topological defects would be observed; and only in the case of external field considerably exceeding $h_{DW} = 0.7085$ domain walls go up to the corner. This

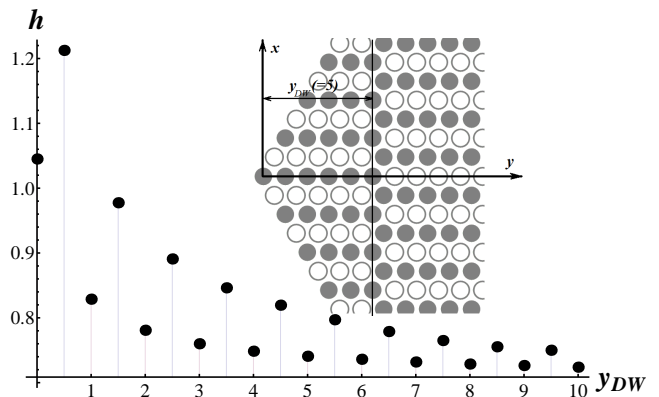


Рис. 8: Dependence of the field of line formation on the distance to the corner of the array.

case is opposite the magnetization process for a square lattice which is initialized on the borders. If we go out of the thermodynamical limit and look at the slow dynamics of the system then we could expect that for the strong external magnetic field (close to h_{120}) the topological defects initially appears close to the corner and then drifts to the volume due to the aforesaid reduction of the potential barrier.

VI. GROUND STATE FOR FINITE ARRAYS

An analysis of finite arrays was accomplished numerically, with usage of the same Monte-Carlo procedure as described above for infinite systems. The different shapes, either fully consistent with the geometry of triangular lattice (bordered by dense lines of magnetic dots only, like rhombus, triangle, hexagon) or less consistent with underlying lattice (rectangle, circle) shows a big variety of the magnetic structures.

A. Zero magnetic field

As has been found in the previous section, the simple two-sublattice AFM survives near the border of semi-infinite system, with one essential exception: the border of the type of a dense line with parallel magnetic moments is unstable at zero magnetic field. This instability is crucial for an understanding of the formation of the ground state for finite samples bordered by dense lines only (rhombus, triangle and hexagon).

1. rhombus

The rhombus is the only simple geometrical form of finite array with the simple AFM structure which can be bordered by dense lines for particles with alternating

magnetic moments. Here the three possibilities of orientation of rhombus with respect to the lattice corresponds with three alternating AFM structures present at Fig. 1. For this reason, at zero magnetic field only the rhombus could provides ideal AFM ordering. Numerical analysis confirm this suggestion demonstrating simple two-sublattice structure, with lines from one sublattice inclined by the angle 60° to the border lines, for rhombuses with different sizes and shapes, see an example on the Fig. 9.

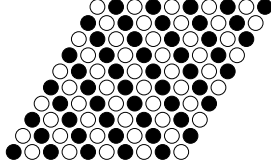


Рис. 9: Minimal configuration for a rhombus-shaped finite system at zero magnetic field.

2. triangle and hexagon

The samples shaped as a right triangle or a hexagon with ideal AFM structure cannot satisfy the above condition, an absence of the border line from one sublattice. This leads to appearance of some kind of domain structures in the ground state, see Fig. 10.

For triangular sample, the domain structure with two AFM domains turned at the angle of 60° , is present in the ground state. For the hexagon, the minimal configuration consists on three domains, where the sublattice lines are inclined on 120° . The three domain walls in this structure are going out from the corners and coming together at the center of the sample in such way that the structure has the three-fold symmetry axis, see right part of the Fig. 10.

It is worth noting here that the corresponding domain walls have zero energy in the nearest-neighbor approximation, but the energy losses caused by the walls are small for long-ranged dipole interaction as well. For these samples most of the «bulk» sites have the optimal «2-4» neighborhood, with the only one exception: The

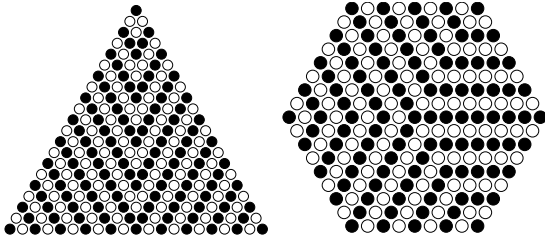


Рис. 10: minimal configurations for the triangle with the side 21 (left) and for the hexagon with the side 8 (right).

«2-4» rule is broken for the central site of hexagonal sample. In the nearest-neighbor approximation, the effective field on the central site equals to zero, and the central magnetic moment is very sensitive to the application of the magnetic field. For large hexagonal sample with real magnetic dipole interaction, the field of the turn of this moment is also small,

$$H_{hex} = -(6\sigma_{60}^{asym} + 3\xi_1 + 3\xi_{-1})\frac{m_0}{a^3} = 0.428266\frac{m_0}{a^3}, \quad (21)$$

and the magnetization reversal is starting by the turn of the central magnetic moment. But detailed analysis shows that the field for the turn of the moments neighboring the center is growing fast with the distance to the center, and the magnetization reversal is following the same scenario as for infinite or semi-infinite systems, see the next subsection.

3. rectangle

For trivial geometrical conditions, the rectangular sample can have only one pair of sides (two parallel sides) parallel to elementary translation vector; these sides have standard AFM structure with interlacing of up and down magnetic moments, see Fig. 11. Two other pair of borders of rectangular are parallel lines of sites with relatively low density within the line (the distance between the sites equals to $a\sqrt{3} \simeq 1.73a$), but with a small enough distance $(a/2)\sqrt{3} < a$ with the next equivalent lines. The preferable type of ordering for two such lines corresponds to the parallel alignment of the magnetic moments within the line with the antiparallel orientation for neighboring lines («2-0» type surface state) whereas the ideal AFM structure leads to much less favorable «1-1» type surface state. For this reason, one can expect the deformation of the ideal AFM structure in a rectangular sample. The numerical analysis confirms this simple speculation based on nearest-neighbor approximation, see Fig. 11.

The ground state of rectangular sample contains zigzag deformation of the characteristic lines of the ideal AFM structure such that the ideal AFM sign-interlacing distribution is kept at the dense border, with the specific structure of finite half-hexagons on the less dense borders. This structure provides the aforementioned picture of saturated lines parallel to less dense borders with «2-0» type surface state. The zigzag lines are always parallel to the less dense borders, whereas the hexagon surface structure depends on how the long side of rectangular sample is oriented respectively to the elementary translation vector, see Fig. 11(a) and Fig. 11(c) for elongated rectangles and Fig. 11(b) for a square sample.

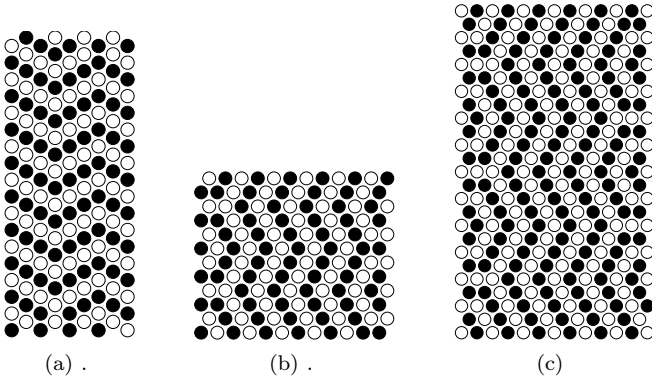


Рис. 11: Minimal configurations for rectangular samples of different shapes; (a) — rectangle, elongated along the elementary translation vector; (b) — square sample, (c) — rectangle, elongated perpendicularly to the elementary translation vector.

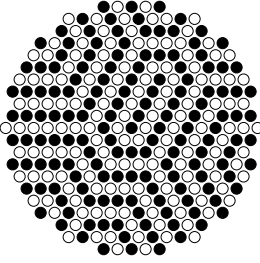


Рис. 12: Ground state magnetic configuration for the circular sample of the radius 9 found by Monte-Carlo simulations.

4. circle

The circular samples are considered here as an example of systems with non-small surface roughnesses. The numerical analysis demonstrates the essential deformations of the ideal AFM structure for such samples, see Fig. 12. Quite non-regular border structure having sites with 3 or 4 nearest neighbors, leads to big variety of the local surface configurations with different numbers of parallel and antiparallel nearest magnetic moments, like «2-1», «3-0» and «3-1» local states. But note that the local AFM structure, in particular, «4-2» condition for the local states, is kept for most bulk sites.

B. Magnetization processes for finite samples.

The magnetization functions for finite systems: hexagon with the side length 8 (215 sites) and square 12×12 (144 sites) are presented on the Fig. 13. The result for infinite system is cited for comparison.

The magnetization function for the finite arrays in many details repeats such a function for infinite system. All typical fields of the structure change are reduced due to long-range nature of the dipole-dipole interaction and

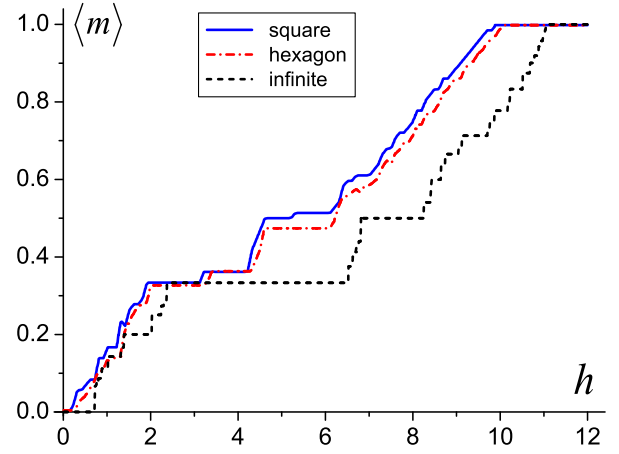


Рис. 13: (color online) Magnetization function for the finite systems; hexagon with the side length 8 (215 sites) and square 12×12 (144 sites), in comparison with that for infinite system.

its cropping on the length of the order of the sample size R . This feature is more strikingly expressed for the saturation field, where the respective sum converges with the distance as R^{-1} , rather than for the field of antiferromagnetic destruction, which evaluates by the rapid convergent alternating sums. At small fields the same the topological domain wall scenario is present, with the orientation of the domain walls consistent with the shape of the sample, see Fig. 14(a). Step-like behavior (plateau behavior) of the function of the infinite system corresponding to the becomes less pronounced in the case of the finite array due to the incommensurateness between the superlattice structure and the shape of the sample. However the period is small for the triangular superlattices of the small parameters ($\sqrt{3}$ и 2) and incommensurateness does not have impact yet. In this case typical plateaus are visible on the magnetization curve and additional fine structure of the form of the low steps appears on them. This fine structure is relating to the change of superstructure contours but not to its reorganization.

As has been shown in Sec. V, the edges of finite array are “weak points” for a single-dot instability, and the values of the instability field for a dot at the vertex of edges are lower than in the bulk, see Eq. (18) and Eq. (19). Thus for a finite sample with the increasing of the external field the saturation starts at the border at lower fields and the area of the superlattice will be reduced. Such behavior is shown on the Fig. 14(b) и Fig. 14(c). As one can see from the Fig. 14, configurations for the hexagon are in the good correspondence with the configuration for the infinite system. The only difference is the presence of saturated dense border lines at high enough fields.

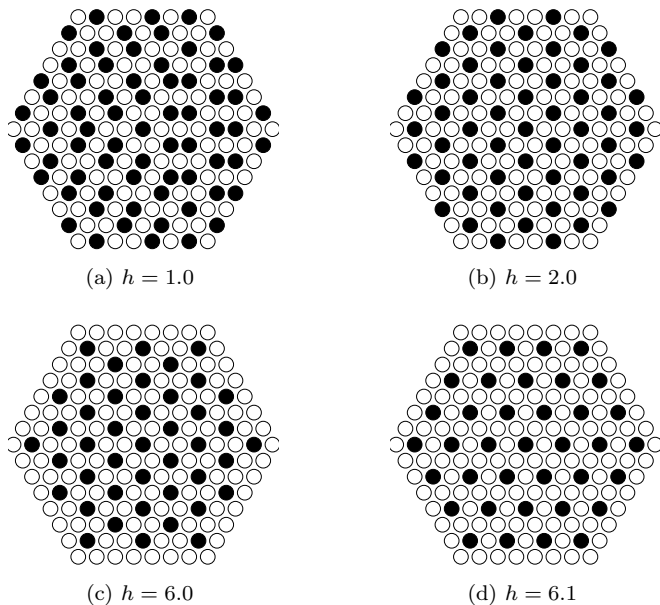


Рис. 14: Magnetic structure for hexagonal sample with the size 7 at some characteristic values of the magnetic field.

VII. DISCUSSION AND CONCLUSIONS

Let us now discuss the general regularities revealed in the behavior two two-dimensional systems with dipolar coupling of Ising magnetic moments, the triangular lattice and the square lattice of magnetic particles. First note that for nearest-neighbors interaction the features of ordering for these two lattices are of principal difference; the square lattice Ising moments at finite temperature shows typical phase transition to the phase with the long range chessboard AFM order, whereas the AFM Ising triangular lattice system still unordered until $T \rightarrow 0$.^{33,34} The reason, well discussed in the literature, is based on the frustrated character of triangular magnets with AFM interaction.³³ The nearest-neighbors Ising AFM system is an extreme example of such feature, because it has topological defects with zero energy, which can lead to destruction of long-range order.^{35,36}

For our case of long-ranged dipolar interaction the role of frustration is not so crucial; it is enough to mention that for a square lattice of Ising moments with dipolar coupling the next-nearest-neighbors in AFM structure are frustrated as well. On the other hand, the topological defect lines having zero energy for triangular lattice nearest-neighbor system gain finite (but small) energy for real dipolar interaction. But the effects of frustration for nearest-neighbors interaction produce an essential difference in the behavior of the systems of interest, magnetic dot arrays with square and triangular lattices.

First let us mention the properties common for both square lattice and triangular lattice. Their ground state at zero field is antiferromagnetic, and the saturated (ferromagnetic) state is present for high enough magnetic

fields. For high magnetic fields, nearly the saturation, the behavior of both lattices is practically the same. The destruction of the saturated state for both lattices happens through creation of a superlattice of reversed magnetic moments, and at $h \rightarrow h_{sat}$ both superlattices are triangular. We can only mention a quantitative difference of the saturation fields, the value for triangular lattice, $11.034m_0/a^3$, is a bit higher than for a square lattice, $H_{sat, square} = 9.033622m_0/a^3$. This difference just reflects the fact that the square lattice is less dense than triangular. But for the region of low fields, corresponding to the destruction of AFM state, and for intermediate fields, where non-saturated states with $\langle m \rangle = (0.2-0.8)m_0$ occurs, the behavior of these two lattices is completely different.

For the square lattice the states with small, but non-zero $\langle m \rangle$ can be obtained from the chessboard AFM structure by reversing the magnetic moments of a small fraction of magnetic dots upward, leaving the remainder undisturbed.¹¹ For a triangular lattice, the destruction of the ideal AFM structure is determined by creation of the system of topological lines (domain walls). The creation of such a single line (or small density of such lines) effects approximately one half of the particles in the system. Thus, this phenomena appears at much lower field (compare the values $2.646m_0/a^3$ and $0.7086m_0/a^3$ for these two lattices) but needs to overcome much higher potential barrier.

For intermediate region of fields, the common property for both lattices is that the ground states are mostly characterized by complicated superlattices with different densities of “up” and “down” magnetic moments. But the process of magnetization for an array with square dot lattice is influenced mainly by an interplay between square and (distorted) triangular superlattices of “down” moments. Such behavior is dictated by a compromise between the optimum of interaction energy (evident for triangular superlattice) and the absence of the distortion energy for square superlattice commensurate with the underlying lattice. In contrast, for a triangular dot array triangular superlattices are optimal from any point of view. Such structures occur at the main regions of field, producing well-defined “shelves”. However, the frustration effects are present for any triangular lattices and superlattices, leading to complicated character of the transition between the states with superlattices of different period, especially small periods like $a\sqrt{3}$ and $2a$.

It is also reasonable to discuss briefly problems that remain beyond the scope of this paper. Of course, the problem of the transition from the out-of-plane (Ising) states to planar states when the magnetic field varies for finite anisotropy for a single dot is of interest. Anisotropy energy for n -th dot can be written as $(1/2)m_0H_{an}(\vec{\sigma}_n \cdot \vec{e}_z)^2$, where the anisotropy field, H_{an} characterizing the strength of the anisotropy energy, is introduced. In fact, this means the construction of a phase diagram on the H, H_{an} plane. One can expect that

Ising states are stable for sufficiently large anisotropy, when the anisotropy energy is comparable with the energy of interaction between neighboring dots, $H_{\text{an}} \geq m_0/a^3$. The analysis of the square lattice corroborates this rule,³⁹ and demonstrates that the Ising states are stable at $H_{\text{an}} \geq 5m_0/a^3$. It is rather difficult to analyze planar states analytically. Our preliminary numerical data indicate that the non-saturated states at small anisotropy correspond to complex noncollinear structures, which are characterized both by significant two-dimensional inhomogeneity with a scale of about the sample size, and by the presence of regions where neighboring magnetic moments are substantially noncollinear, and full description of such states can be

done only numerically. The complete analysis of non-collinear states is evidently far beyond the scope of our article.

acknowledgments

We are thankful to V. G. Bar'yakhtar for useful discussions and help. This work was partly supported by the National Ukrainian Academy of Sciences via grant No. 228-11 and Scientific and Technical Center of Ukraine (STCU), project No. 5210.

-
- * Electronic address: bivanov@i.com.ua
- 1 A. I. Akhiezer, V. G. Bar'yakhtar, and S. V. Peletminskii, *Spin Waves*, North-Holland, Amsterdam (1968), Nauka, Moscow (1967).
 - 2 A. F. Andreev and V. I. Marchenko, *Sov. Phys. Usp.* **23**, 21 (1980).
 - 3 A. Hubert and R. Schafer, *Magnetic domains. The analysis of Magnetic Microstructures*, Springer, Berlin (1998).
 - 4 V. G. Baryakhtar, A. N. Bogdanov, and D. A. Yablonskii, *Sov. Phys.-Uspekhi* **31**, 810 (1988).
 - 5 V. G. Baryakhtar and B. A. Ivanov, *Sov. Phys. JETP* **45** (4), 789 (1977).
 - 6 J. M. Luttinger and L. Tisza, *Phys. Rev.* **70**, 954, 1946.
 - 7 P. I. Belobrov, R. C. Gekht and V. A. Ignatchenko, *Sov. Phys. - JETP* **57**, 636 (1983).
 - 8 J. G. Brankov and D. M. Danchev, *Physica A* **144**, 128 (1987); S. Prakash and C. L. Henley, *Phys. Rev. B* **42**, 6574 (1990).
 - 9 K. Yu. Guslienko, *Appl. Phys. Lett.* **75**, 394 (1999).
 - 10 V. M. Rozenbaum, V. M. Ogenko, and A. A. Chuiko, *Sov. Phys. Usp.* **34**, 883 (1991).
 - 11 J. E. L. Bishop, A. Yu. Galkin and B. A. Ivanov, *Phys. Rev. B* **65**, 174403 (2002).
 - 12 A. Yu. Galkin, B. A. Ivanov and A. Yu. Merkulov, *JETP* **101**, 1106 (2005).
 - 13 A. Yu. Galkin and B. A. Ivanov, *JETP Lett.* **83**, 383 (2006).
 - 14 A. Yu. Galkin, B. A. Ivanov and C. E. Zaspel, *J. Magn. Magn. Mater.* **286**, 351 (2005)
 - 15 A. Yu. Galkin, B. A. Ivanov, and C. E. Zaspel, *Phys. Rev. B* **74**, 144419 (2006).
 - 16 P. V. Bondarenko, A. Yu. Galkin, B. A. Ivanov, and C. E. Zaspel, *Phys. Rev. B* **81**, 224415 (2010).
 - 17 S. V. Maleev, *Sov. Phys. JETP* **43**, 1240 (1976).
 - 18 P. Bruno, *Phys. Rev. B* **43**, 6015 (1991).
 - 19 B. A. Ivanov and E. V. Tartakovskaya, *Phys. Rev. Lett.* **77**, 386 (1996).
 - 20 R. Skomski, *J. Phys.: Condens. Matter* **15**, R841 (2003); *Advanced Magnetic Nanostructures*, edited by D. J. Sellmyer and R. Skomski, (Springer, New York, 2006).
 - 21 B. Hillebrands, C. Mathieu, C. Hartmann, M. Bauer, O. Buettner, S. Riedling, B. Roos, S. O. Demokritov, B. Bartenlian, C. Chappert, D. Decanini, F. Rosseaux, E. Cambril, A. Muller, B. Hoffmann, and U. Hartmann, *J. Magn. Magn. Mater.* **175**, 10 (1997).
 - 22 C. Miramond, C. Fermon, F. Rousseaux, D. Decanini and F. Carcenac, *J. Magn. Magn. Mat.* **165**, 500 (1997).
 - 23 E. F. Wassermann, M. Thielen, S. Kirsch, A. Polmann, H. Weinforth, and A. Carl, *J. Appl. Phys.* **83**, 1753 (1998).
 - 24 K. Runge, T. Nozaki, U. Okami, H. Miyajima, B. Pannetier, T. Matsuda and A. Tonomura, *J. Appl. Phys.* **79**, 5075 (1996).
 - 25 R. P. Cowburn, D. K. Koltsov, A. O. Adeyeye, M. E. Welland, and D. M. Tricker, *Phys. Rev. Lett.* **83**, 1042 (1999).
 - 26 P. D. Ye, D. Weiss, K. von Klitzing, K. Eberl and H. Nickel, *Appl. Phys. Lett.* **67**, 1441 (1995).
 - 27 C. B. Murrey, D. Weller, L. Folks, and A. Moser, *Science* **287**, 198 (2000).
 - 28 S. Y. Chou, M. S. Wei, P. R. Krauss, and P. B. Fischer, *J. Appl. Phys.* **76**, 6673 (1994).
 - 29 G. Meier, M. Kleiber, D. Grundler, D. Heitmann, and R. Wiesendanger, *Appl. Phys. Lett.* **72**, 2168 (1998).
 - 30 C. A. Ross, M. Hwang, M. Shima, J. Y. Cheng, M. Farhoud, T. A. Savas, H. I. Smith, W. Schwarzacher, F. M. Ross, M. Redjda, and F. B. Humphrey, *Phys. Rev. B* **65**, 144417 (2002).
 - 31 V. V. Kruglyak, S. O. Demokritov, and D. Grundler, *Journ. of Phys. D-Applied Physics*, **43**, 264001 (2010).
 - 32 D. J. Sellmyer, M. Zheng and R. Skomski, *J. Phys.: Condens. Matter* **13**, R433 (2001).
 - 33 R. S. Gekht, *Sov. Phys. Usp.* **32**, 871 (1989).
 - 34 G. H. Wannier, *Phys. Rev.* **79**, 357 (1950); R. M. F. Houtappel, *Physica* **16**, 425 (1950); G. H. Wannier, *Phys. Rev. B* **7**, 5017 (1973).
 - 35 S. E. Korshunov, *Phys. Rev. B* **71**, 174501 (2005).
 - 36 S. E. Korshunov, *Phys.—Usp.* **49** (3), 225 (2006).
 - 37 B. A. Ivanov and V. E. Kireev, *JETP Lett.* **90**, 750 (2009).
 - 38 P. A. Slotte and P. C. Hemmer, *J. Phys. C* **17**, 4645 (1984).
 - 39 P. V. Bondarenko, A. Yu. Galkin, and B. A. Ivanov, *JETP* **112**, 986 (2011).
 - 40 S. Kirkpatrick, C. D. Gelatt, Jr. and M. P. Vecchi, *Science* **220**, no. 4598, 671 (1983).
 - 41 V. Černý, *Journal of Optimization Theory and Applications* **45**, 41 (1985)
 - 42 M. E. J. Newman, G. T. Barkema, *Monte Carlo Methods in Statistical Physics*, (Oxford University Press, USA, 1999).

Appendix. Numerical method description

To find the global minimum of the energy of the system the Monte-Carlo approach with a simulated annealing (MC-SA) method was used, see original articles Refs. 40, 41 and the textbook Ref. 42. For MC-SA realization, first, the random initial configuration was selected. Every iteration of the MC-SA method consists of N moment reversal attempts on the random site, where N is the site number in the sample. The main idea of simulated annealing is that the probability of the reversal is non-zero even if the energy is growing after this reversal; otherwise, the system with a high probability will be “frozen” in some local minimum. The probability depends not only on energy gain for reversal, which equals to Hm_0 (H is a value of the field created by other dots on a given) but also on a global time-varying parameter T called the *temperature*. If the reversal is favorable in energy, the moment is always reversed, irrespective of the temperature. But even if the reversal is unfavorable, the non-zero probability of reversal is chosen as follows: flip-over takes place if $Hm_0 < T|\log p|$, where T is the current value of temperature, p is a random value generated in the range $0 < p \leq 1$. Here the parameter temperature determines the strategy of the minimization: for large T , the evolution is sensitive to coarser energy variations, while it is sensitive to finer energy variations when T is small. Thus the meaning of the temperature is the same as for annealing in metallurgy involving initial heating and controlled cooling of a material thereby avoiding defect formation.

The temperature is changing according to the quantity of full steps of MC-SA of the sample n as follows, $T = T_0 \min[\kappa, (n_0/n)^\alpha]$. Here the parameter T_0 was

chosen as $(0.2-0.4)m_0^2/a^3$, and the cutoff parameter κ was equal to $\kappa = 3.0$ such that the initial temperature was high enough compared with the interaction energy. The optimal values of other parameter are defined by the trial runs; n_0 was equal to $10^4 - 5 \cdot 10^4$ and the value of the α -index was taken 1/4 or 1/5.

The temperature decreases with the process evolution and magnetization reversals take place more rarely with decreasing energy. The process was stopped if the energy did not become less than the previous minimum during the previous $10n_0$ iterations. Then the next random configuration was generated and the process was repeated. Looking at the energies of minimal configurations for every run one can estimate the probability that such a configuration corresponds to the true minimum. For example, almost all processes of the cooling go through the same minimum far from the regions of the parameters which correspond to the transition between different states.

For the configurations on the infinite lattice we took the rhombuses with the consecutive increasing periods up to 16×16 and used periodic boundary conditions. The energy of the configuration was recalculated to the energy per one dot thereby making possible the comparison of the results for the different periods. A rhombus was selected to admit the maximum possible configuration set to consideration, but minimal configurations often have higher symmetry.

A similar approach was used to build a magnetization function. Firstly, all ranges of the fields were passed with large intervals and small periods of the rhombuses. After that the regions of the structure rebuilding were detected, where the field intervals were taken smaller and periods were taken larger.